13C NMR Parameters of Disordered Carbons: Atomistic Simulations, DFT Calculations, and Experimental Results

Alan Ambrozio, Jean-Marc Leyssale, Roland J-M Pellenq, Fabio Al de Souza, Gérard L. Vignoles, Wanderla L Scopel, Jair Cc Freitas

^{13}C NMR Parameters of Disordered Carbons: Atomistic Simulations, DFT Calculations and Experimental Results

Alan R. Ambrozio,[†,‡] Jean-Marc Leyssale,[*,‡,¶] Roland J.-M. Pellenq,[‡,§] Fábio A. L. de Souza,[∥] Gérard L. Vignoles,[⊥] Wanderlã L. Scopel,[†] and Jair C. C. Freitas[*,†]

Laboratory of Carbon and Ceramic Materials, Department of Physics, Federal University of Espírito Santo (UFES), Av. Fernando Ferrari, 514, 29075-910, Vitória, ES, Brazil., CNRS/MIT/Aix Marseille Univ. joint lab "MultiScale Materials Science for Energy and Environmen", IRL 3466, Massachusetts Institute of Technology, 77 Massachusetts Avenue, Cambridge, MA 02139, USA, Institut des Sciences Moléculaires, Université de Bordeaux, CNRS UMR 5255, 351 Cours de la Libération, 33405 Talence, France., Department of Civil and Environmental Engineering, Massachusetts Institute of Technology, Cambridge, MA 02139, USA., Federal Institute of Education, Science and Technology of Espírito Santo, Ibatiba/ES, Brazil., and Laboratoire des Composites ThermoStructuraux (LCTS), UMR-5801 CNRS/UB/CEA/Safran, Université de Bordeaux, 3 Allée de La Boétie, 33600 Pessac, France.

E-mail: jean-marc.leyssale@u-bordeaux.fr; jairccfreitas@yahoo.com.br

Abstract

The ^{13}C NMR chemical shifts corresponding to different sites in atomistic models of disordered carbons were computed at different H contents by employing DFT calculations. Structural models were generated by molecular dynamics simulations and validated by the pair distribution functions; further bonding analyses were carried out to determine the amount of sp^3 and sp^2 carbons in the structures. Specifically, the obtained results allow the distinction of the chemical shifts associated with different types of carbon sites, with different hybridization states and bonded or not to a hydrogen atom. The calculated NMR spectra show excellent agreement with experimental data and are thus useful to identify local structural features of disordered carbons.

Introduction

Carbon materials have been extensively investigated along the past years because of their unique properties at different allotropies, for instance, graphite-like materials - graphene, nanographites, pyrocarbons, and disordered carbons - carbon blacks, amorphous carbons, activated carbons, diamond-like materials, fullerenes, carbon nanotubes, kerogens and others. In many of these studies, different structural models have been employed for the description of the physical properties of carbon materials.[1] Generally, the proposed models are validated by confronting the predicted properties against experimental results derived from diffraction techniques (e.g., X-ray and neutron diffraction) as well as spectroscopic (e.g., Raman and

---

*To whom correspondence should be addressed

†Laboratory of Carbon and Ceramic Materials, Department of Physics, Federal University of Espírito Santo (UFES), Av. Fernando Ferrari, 514, 29075-910, Vitória, ES, Brazil.

‡CNRS/MIT/Aix Marseille Univ. joint lab "MultiScale Materials Science for Energy and Environmen", IRL 3466, Massachusetts Institute of Technology, 77 Massachusetts Avenue, Cambridge, MA 02139, USA

¶Institut des Sciences Moléculaires, Université de Bordeaux, CNRS UMR 5255, 351 Cours de la Libération, 33405 Talence, France.

§Department of Civil and Environmental Engineering, Massachusetts Institute of Technology, Cambridge, MA 02139, USA.

‖Federal Institute of Education, Science and Technology of Espírito Santo, Ibatiba/ES, Brazil.

⊥Laboratoire des Composites ThermoStructuraux (LCTS), UMR-5801 CNRS/UB/CEA/Safran, Université de Bordeaux, 3 Allée de La Boétie, 33600 Pessac, France.

nuclear magnetic resonance spectroscopy) or microscopic (e.g., transmission electron microscopy) methods.[2–4] There is a wide range of computational techniques for generating satisfactory structural models for carbon materials, which are mainly based on molecular dynamics (MD), Monte Carlo or a combination of both.[5,6] In particular, MD has proven to be a useful tool for generating appropriate models of disordered carbon materials.[2–4,7]

Among the important properties of carbon materials, the nuclear magnetic resonance (NMR) chemical shielding is particularly useful due its sensitivity to the local chemical environment around the probe nuclei. Moreover, the components of the NMR chemical shielding tensor can be obtained from atomistic models and confronted directly with experimental data; consequently, measurements and calculations of the components of the chemical shielding tensor are of high interest both for crystalline and disordered materials.[8–10] Especially, the use of NMR to probe the local bonding structure can be an adequate complement to diffraction techniques (e.g, X-ray, electron or neutron diffraction), which are more suited to probe the average local environments or the medium to long range order in the material. Recent theoretical reports have used first-principles calculations based on the density functional theory (DFT) to establish correlations between the shielding tensor and structural features of carbon nanotubes,[11] graphite oxide,[12] graphene and graphitic materials.[13,14]

Amorphous hydrogenated carbons have been extensively studied in the past decades due to their interesting mechanical and tribological properties, which have promising applications. These properties are dependent on chemical and structural features such as the H content in the material and the amount of atoms with sp and sp^3 hybridization.[15–17] Solid-state ^{13}C NMR methods have been widely used in studies of amorphous carbons, especially regarding the quantitative evaluation of the sp^2/sp^3 ratio. In fact, this ratio is a particularly important property that can be easily obtained from ^{13}C NMR spectra, considering the clear distinction in the chemical shift ranges corresponding to sp^2 and sp^3 carbons.[18] As an example, Pan $et\ al.$[19] estimated that just ca. 1.5% of the carbon content in an amorphous carbon film could be detected in ^{13}C NMR spectra obtained with ^1H-^{13}C cross polariza-

tion (CP),[18] concluding that this contribution was due to sp^2- and sp^3-like carbon atoms located at the edges of the amorphous carbon network. More recently, Cho $et\ al.$.[20] studied the chemical changes occurring in amorphous hydrogenated carbon films with different H contents, using a combination of NMR methods including spectral editing. Regarding the calculation of NMR properties, Mauri and co-workers[21] used systems with atomic geometries generated by MD to compute (by DFT) the chemical shielding and predict the ^1H and ^{13}C NMR spectra of amorphous carbon samples with different densities and H contents. The comparison of these predictions with experimental results allowed the interpretation of NMR spectra recorded for samples with similar properties, making possible the identification of contributions coming from 3-fold and 4-fold coordinated carbon atoms. A similar approach was followed by Alam $et\ al.$[22] in a study about tetrahedral amorphous carbon films.

In the recent work by Bousige $et\ al.$,[7] a panel of realistic molecular models of mature and immature kerogens has been reconstructed using a hybrid experimental-simulation method. These models have been shown to accurately reproduce the diffraction properties of the materials (e.g., the pair distribution functions derived from X-ray diffraction) as well as the vibrational density of states from inelastic neutron scattering.

However, the NMR properties of models containing several thousands of atoms, as it is in general the case of MD-derived models, cannot be directly predicted by usual cubic scaling DFT calculations, which typically cannot deal with more than a few hundreds of atoms.[23,24] Instead, the present work proposes an approach in which relatively small-sized models are produced by MD simulations and their NMR properties are predicted by DFT calculations, so that the individual NMR spectral features associated with the different types of chemical environments present in the materials can be determined. More specifically, this work describes the calculation of the NMR chemical shifts of disordered hydrogenated carbons presenting different H/C ratios, using a combination of MD and DFT simulations. The MD simulations were employed to generate the structural models of hydrogenated disordered carbons. From MD simulations, the pair distribution functions (PDF) and the fractions of

carbon atoms exhibiting sp, sp^2 and sp^3 hybridizations were obtained for each structural model. DFT calculations were then carried out in order to determine the ^1H and ^{13}C NMR shielding tensors associated with each atomic site and these parameters were related with the type of hybridization as well as the hydrogen content. The results obtained by these calculations were rationalized considering the H/C ratios of each system and were also confronted with the experimental results available for systems with similar chemical compositions.

Computational Details

Generation of atomic model - MD simulations

Following recent work by Obliger *et al.*,[25] small scale atomistic models of hydrogen-containing disordered carbons were generated using standard liquid quench MD procedure and the last generation of ReaxFF potential called ReaxFF$_{C-2013}$,[26] which can describe the chemistry and dynamics of carbon condensed phases more accurately than earlier versions of the ReaxFF potential.[27,28] In order to maximize the bonding between H and C atoms, attractive $H-H$ interactions were switched off by setting to zero the value of the dissociation energy parameter of the ReaxFF potential (for more details see refs.[26–28]). In this approach, a simple cubic lattice is generated at the suited density with a random assignation of C and H atoms to the lattice sites. This lattice is then melted to form a well-equilibrated liquid phase using MD simulation at constant number of atoms N, volume V and temperature T during 100 ps. A value of 6000 K is used for the temperature. In the second step, the liquid is quenched at constant volume by applying a linear temperature ramp, obtained by updating the target temperature of the thermostat at every time step, to bring it down to 300 K at a specified rate. At the end of the quench, the system has formed a connected solid phase and, possibly, some small hydrocarbon molecules trapped into the skeleton porous structure. Such fluid molecules are removed from the system and the solid phase is relaxed at 300 K and zero pressure using 10 ps of MD in the isothermal-isobaric (NPT) ensemble. During this step,

most residual stress is released. Varying the density, composition and quenching rate allows the production of atomistic models with different chemical composition, texture and porosity.

Three initial cubic lattices of 216 atoms were considered with same initial density of 1.9 g/cm^3 and different compositions. System A: $H/C = 0.05$ and $L = 12.95$ Å; system B: $H/C = 1.0$ and $L = 10.71$ Å; system C: $H/C = 1.86$ and $L = 9.72$ Å. Also, four different quenching rates were considered for each system: 100, 50, 25 and 5 K/ps. All simulations were performed with the open source Large-scale Atomic/Molecular Massively Parallel Simulator (LAMMPS) package.[29] Equations of motions were integrated using the velocity Verlet scheme[30] with a time step of 0.1 fs. Nosé-Hoover thermostat and barostat[31,32] were used to fix temperature and pressure using time constants of 200 and 50 fs for the barostat and thermostat, respectively. The barostat was applied independently to each diagonal element of the pressure tensor, changing the shape of the parallel cell from cubic to orthorhombic, yet remaining close to cubic.

DFT calculations

The Quantum Espresso (QE) package[33] was employed to calculate the NMR chemical shielding tensor using the gauge-including projector-augmented wave (GIPAW) method[34] as implemented in the QE Version 5.1. The GIPAW method is based on an extension of the projector augmented-wave (PAW) approach of Blöchl[35] and on previous methods proposed by Mauri *et al.*[21,36,37]

The NMR DFT calculations involve 3 steps: geometry optimization, electronic relaxation (i.e., finding the electronic ground state) and calculation of NMR shielding. The plane-waves method was used to expand the wavefunctions. In all these calculations, the generalized gradient approximation of Perdew-Burke-Ernzerhof (GGA-PBE)[38] and the norm conserving Troullier-Martins pseudopotentials[39] with GIPAW reconstruction were used. The van der Waals interaction was described following the DFT-D2 method.[40]

The energy cutoff was set to be 1088 eV, following the work of de Souza *et al.*,[14] who

analyzed the convergence of NMR shielding parameters calculated for benzene, graphite and graphene; these systems thus involve the same atomic species as the systems analyzed in the present study. All the structures were relaxed keeping the supercell free to change both in shape and volume until the forces acting on each site achieved the convergence criteria ($< 0.01\ eV/\text{Å}$). For large systems such as those used in the present work, a $2 \times 2 \times 2$ grid of k-points was observed to be enough to obtain reliable results.

The GIPAW method was used to calculate the NMR shielding tensor corresponding to each atomic C site of the full relaxed geometries. In order to compare the calculated values with experimental results, from the calculated components of the shielding tensor (σ_{ij}) in its principal axis system, the isotropic shielding is computed as follows:

$$\sigma_G^{(iso)} = \frac{1}{3}(\sigma_{11} + \sigma_{22} + \sigma_{33}). \tag{1}$$

Next, the isotropic shieldings were converted to chemical shifts by the expression:

$$\delta_{G/TMS} = -[\sigma_G - \sigma_{benzene}^{(iso)}] + \delta_{benzene/TMS}, \tag{2}$$

where $\sigma_G^{(iso)}$ and $\sigma_{benzene}^{iso}$ stand for the isotropic shielding for a given carbon site belonging to the system under study and for the isolated benzene molecule. In this work, all the calculated chemical shifts were reported using the isolated benzene molecule as an intermediate reference. As discussed in previous studies,[11,14,41] the benzene molecule contains carbon and hydrogen atoms arranged in a way somewhat similar to the local chemical arrangement found in most disordered carbon materials; thus, the choice of this intermediate chemical shift reference is expected to lead to the cancellation of systematic errors present in the DFT calculations. The parameter $\delta_{benzene/TMS}$ is the experimental chemical shift of benzene in the gas phase with respect to liquid tetramethylsilane (TMS), which is typically used as the primary reference for ^{13}C NMR. The experimental value $\delta_{benzene/TMS} = 126.9\ ppm$[42,43] and the theoretical one $\sigma_{benzene} = 38.8\ ppm$[14] were adopted herein. Hence, chemical shifts

calculated in this work through eq. 2 can be directly compared to other results obtained using liquid TMS as the shift reference.

Experimental Methods

In order to illustrate how the simulated systems and the calculated NMR spectra compare to real cases, ^{13}C NMR experiments were performed for selected materials exhibiting chemical features somewhat similar to the simulated systems. The samples chosen for these experiments (listed in decreasing order of H/C atomic ratio) included a petroleum asphaltene sample (with $H/C = 1.1$),[44] a peat-derived char (heat treatment temperature of 350 °C, with $H/C = 0.69$)[45] and a pyrocarbon of the regenerative laminar (ReL) type, with $H/C = 0.026$, prepared by chemical vapor deposition (CVD).[46]

The ^{13}C NMR spectra were recorded at 9.4 T (100.52 MHz frequency) at room temperature in a Varian/Agilent VNMR 400 MHz spectrometer, using a triple-resonance probehead; the powdered samples were packed into 4 mm diameter zirconia rotors for magic angle spinning (MAS) experiments at the frequency of 14 kHz. For the materials with reasonable ($\sim 5 - 10 \ wt.\%$) hydrogen content (asphaltene and peat char samples), the experiments were conducted with ^{1}H-^{13}C cross polarization (CP), using a ^{1}H $\pi/2$ excitation pulse of 3.6 μs, a recycle delay of 5 s and a contact time of 1.0 ms. The ^{13}C NMR spectrum of the hydrogen-poor pyrocarbon sample was recorded using a spin-echo sequence, with $\pi/2$ and π pulses with durations of 4.3 and 8.6 μs, respectively, an interpulse delay corresponding to 4 rotor periods (ca. 288 μs) and a recycle delay of 15 s. All spectra were obtained by Fourier transform of the free induction decays (FIDs), with the chemical shifts, expressed in parts per million (ppm), externally referenced to TMS.

Results and Discussion

Atomistic models from liquid quench MD

Models were generated for three initial systems of 216 atoms, denoted in this work as systems A, B and C, at the same density of 1.9 g/cm^3, as shown in Table 1. The main difference among these systems is their initial H/C ratios, with values of 0.05, 1.00 and 1.86 corresponding to systems A, B and C, respectively. For each system, different quenching rates were tested: 100, 50, 25 and 5 K/ps. The final obtained structures were found to depend significantly on the value of the quenching rate, with the most reliable results achieved for the lowest quenching rate; for instance, in the case of system A, the formation of graphene-like domains with a PDF compatible with the interatomic distances of graphene-based materials (to be discussed later) was only observed with the quenching rate of 5 K/ps. Therefore, herein only the results obtained for the systems generated using the lowest quenching rate are presented, which are assumed to correspond to the situation closest to thermal equilibrium.

Table 1: Initial and final number of atoms, composition and density corresponding to systems A, B, C cooled at 5 K/ps.

System Label	Number of atoms Initial/Final	H/C ratio Initial/Final	Density (g/cm^3) Initial/Final
A	216/216	0.05/0.05	1.90/1.90
B	216/193	1.00/0.87	1.90/1.46
C	216/170	1.86/1.57	1.90/1.27

At the end of the quench all the systems have formed a covalent solid phase, although some small hydrocarbon molecules could also be observed, especially for systems B and C (which have higher H/C ratios). As mentioned before, these trapped molecules were removed and the system was relaxed at room temperature and zero pressure using MD in the isothermal-isobaric (NPT) ensemble. Snapshots of the three relaxed systems are shown in Figure 1, whereas their initial/final number of atoms, H/C ratios and densities are given in Table 1.

Figure1-(a) shows that model A has typical features of a pyrocarbon, a non-porous, highly
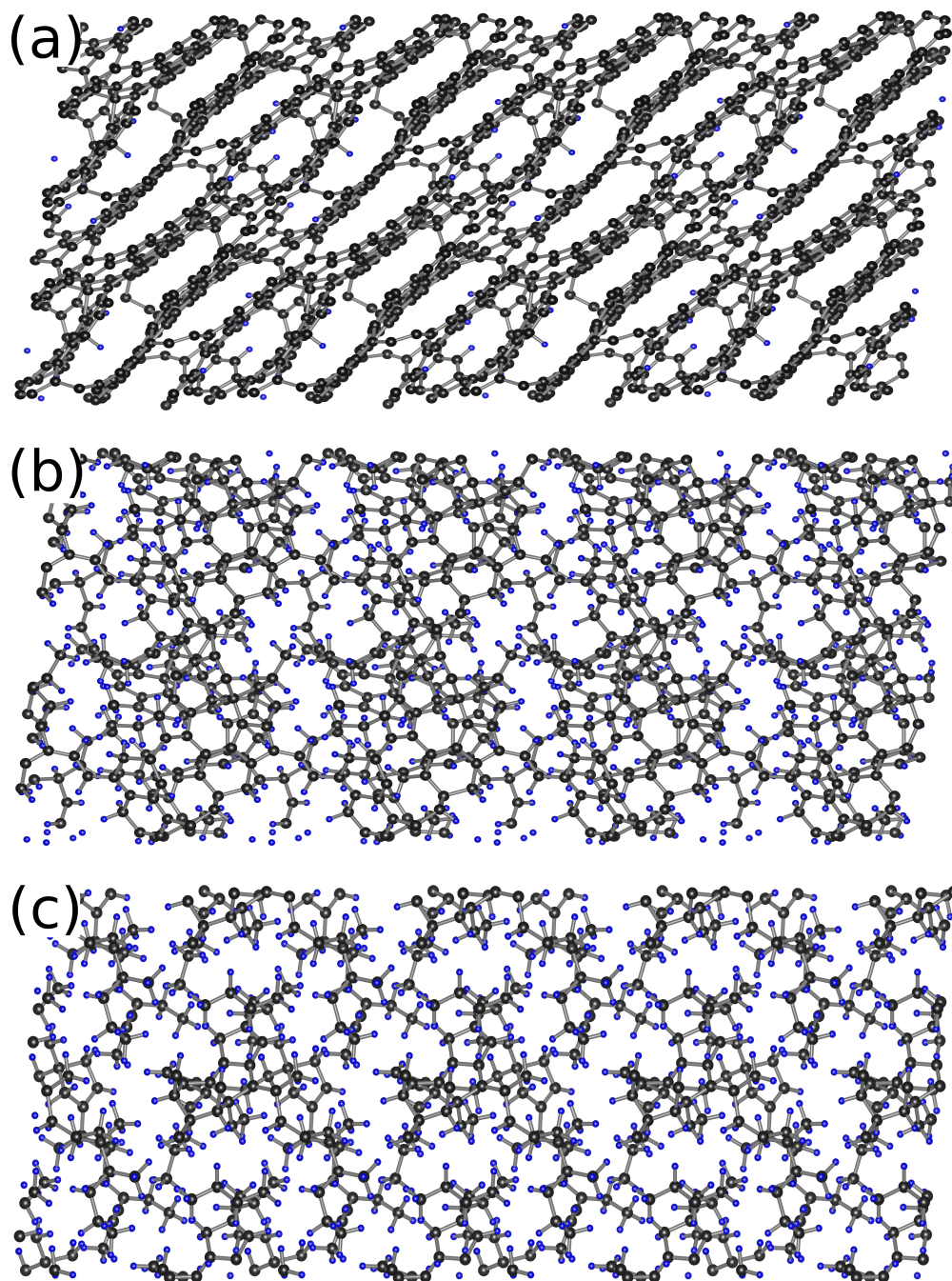
Figure 1: Snapshots of systems (a) A, (b) B and (c) C cooled at 5 K/ps. Carbon (hydrogen) atoms are colored in grey (blue). All systems have been replicated 3 and 2 times along the horizontal and vertical directions, respectively, to ease visualisation.

anisotropic pre-graphitic (or quasi-graphitic) material with distinguishable nanometer-sized graphene-like domains.[2] This is confirmed by the analysis of the PDF obtained for this system, shown in Figure 2, where the normalized distribution of interatomic distances ex-

hibits an intense first peak centered at 1.42 Å, which agrees well with the expected sp^2 bond length.[47,48] The second peak centered at 2.48 Å also reproduces typical second nearest neighbor distances (2.49 ± 0.03 Å) observed in carbon materials composed of graphene-like domains.[49] The existence of correlations up to large distances is also observed in the PDF of system A. Moreover, the analysis of the local chemical environments in the relaxed systems (given in Table 2) shows that 96% of the carbon atoms correspond to threefold bonding (sp^2 hybridization) in the case of system A, which confirms the graphitic nature of this system. Indeed, the X-ray PDFs of nanoporous carbons consisting primarily of sp^2-hybridized car-bon sheets with hexagonal bonding were experimentally determined in ref.,[47] standing in excellent agreement with the PDF obtained in the present work for system A. Additionally, in ref.[48] the PDFs of both rough laminar and smooth laminar pyrocarbons were determined by neutron diffraction experiments, leading to the conclusion that the short-range structure is similar to that of graphite, with the first three neighbors located at distances of 1.42, 2.46 and 2.83 Å. These values are very similar to the C–C bond distances obtained from the analysis of the PDF of system A (Figure 2), which are respectively equal to 1.42, 2.48 and 2.80 Å.

Conversely, systems B and C have much lower densities and almost do not contain any aromatic rings. Their H/C ratios of 0.87 and 1.57 are found in the range of values corresponding to disordered carbon materials exhibiting significant hydrogen content, such as low-rank coals, low-temperature chars, asphaltenes and immature kerogens.[7,50,51] System B shows an almost evenly mixed sp^2/sp^3 hybridization, as revealed by the bi-modal first peak of the PDF (Figure 2) and by the detailed bonding analysis (Table 2). These results can be compared with *ab initio* MD (AIMD) simulations[52] of a hydrogenated amorphous carbon (a-C:H) with an atomic H/C ratio of 0.19, consisting of about 56% fourfold, 41% threefold and a small fraction of twofold coordinated carbon sites, which are fractions similar to the ones found here for system B (see Table 2): 47, 52 and $\sim$ 1%, respectively. The higher fraction of fourfold sites in the system discussed in ref.[52] is consistent with its higher density (2.6

Table 2: Fractions of carbon atoms exhibiting different chemical environments and hybridization types for systems A, B and C. The symbol $C - C_nH_m$ denotes a carbon atom directly bonded to n C atoms and m H atoms. The total fractions of 4-, 3- and 2-fold coordinated carbon atoms for each system are shown in the bottom. The predicted ^{13}C NMR chemical shift range for each chemical environment is also presented.

Chemical Environments	System			Chemical Shift Range (ppm)
$C - C_nH_m$	A	B	C	
$C - C_4$	0.00	7.77	7.57	25 - 105
$C - C_3H$	0.49	12.62	13.64	25 - 75
$C - C_2H_2$	0.00	17.47	33.33	15 - 65
$C - CH_3$	0.00	8.74	22.73	0 - 65
$C - C_3$	91.75	39.81	13.63	85 - 185
$C - C_2H$	4.36	11.65	6.06	85 - 185
$C - CH_2$	0.00	0.97	1.52	105 - 125
$C - C_2$	3.40	0.97	1.52	95 - 135
Coordination Number	A	B	C	
4-fold	0.49	46.60	77.27	0 - 105
3-fold	96.11	52.43	21.21	85 - 185
2-fold	3.40	0.97	1.52	95 - 135

g/cm^3) in comparison with the density of system B here described (1.46 g/cm^3). Moreover, the PDF obtained for the $a - C : H$ sample in ref.[52] exhibited a first peak with two maxima, the first one corresponding to a C-C bond length slightly smaller in comparison to graphite and the second one corresponding to the C-C distance found in crystalline diamond; second neighbors were located at distances centered around 2.6 Å. These results are thus in excellent agreement with the PDF computed for system B, as shown in Figure 2. Furthermore, the results obtained either with the present approach or with the AIMD method are in good agreement with the PDFs derived from neutron scattering experiments conducted in a-C:H samples.[53]

As for system C, the analysis presented in Table 2 shows that it mostly contains sp^3 carbon atoms (roughly 77%), a good part of which being bonded to two C atoms and two H atoms (C-C_2H_2), which is typical of alkyl chains, as in polyethylene. This is consistent with the PDF computed for this system showing a first peak at 1.58Å, which is the typical sp^3 C-C bond length.[54,55]
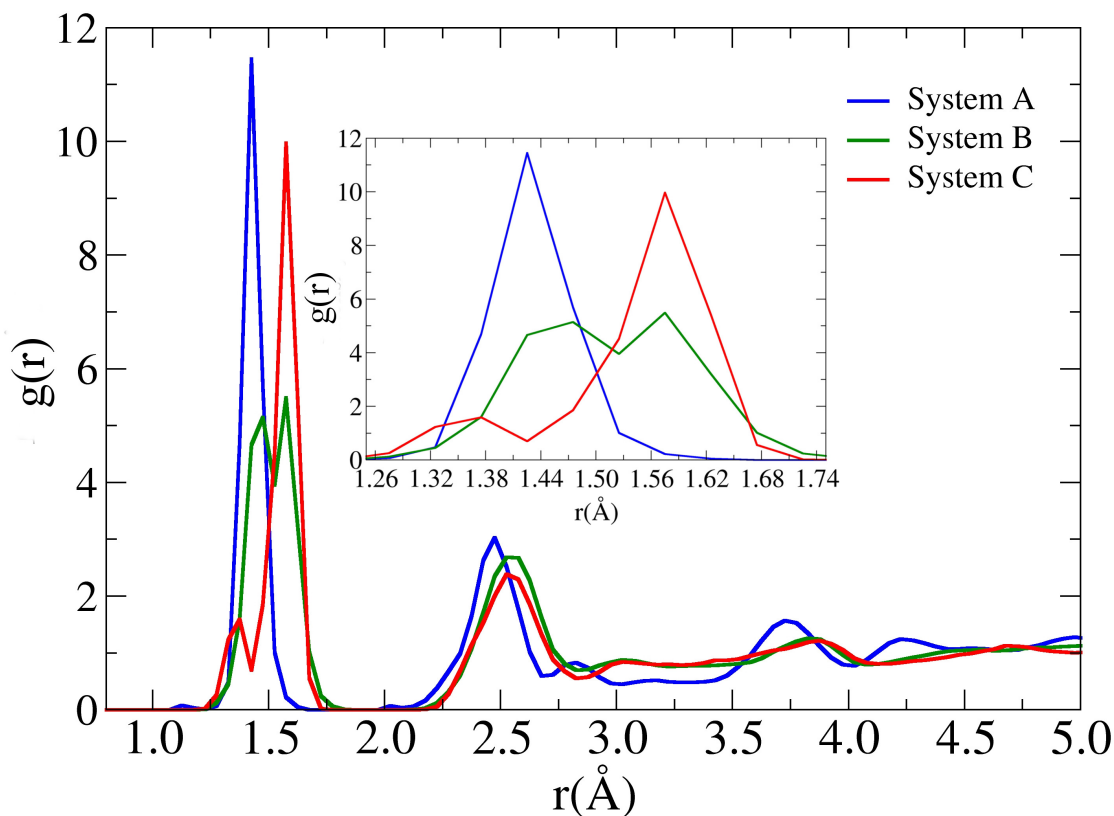
Figure 2: Calculated PDFs for systems A, B and C. The inset shows a zoom in the region around the first peak.

DFT calculations of ^{13}C NMR chemical shifts

The solid-state ^{13}C NMR spectra of most carbon materials (including coals, chars, asphaltenes, amorphous carbons and graphitic materials, among others) are generally composed of two distinct sets of signals at different chemical shift ranges: aliphatic groups (involving carbon atoms with sp^3 hybridization) give signals with isotropic chemical shifts typically between 0 and 90 ppm, whereas aromatic groups (and other groups also involving carbon atoms with sp^2 hybridization) are associated with signals in the chemical shift range $110 - 160$ ppm.[18] These chemical shifts (i.e., the corresponding peak positions in the NMR spectra) are just slightly affected by structural details in different types of amorphous hydrogenated carbon films, as discussed in many previous works.[17,19,20,22,56]

The predicted ^{13}C NMR spectra obtained from the calculated isotropic chemical shifts
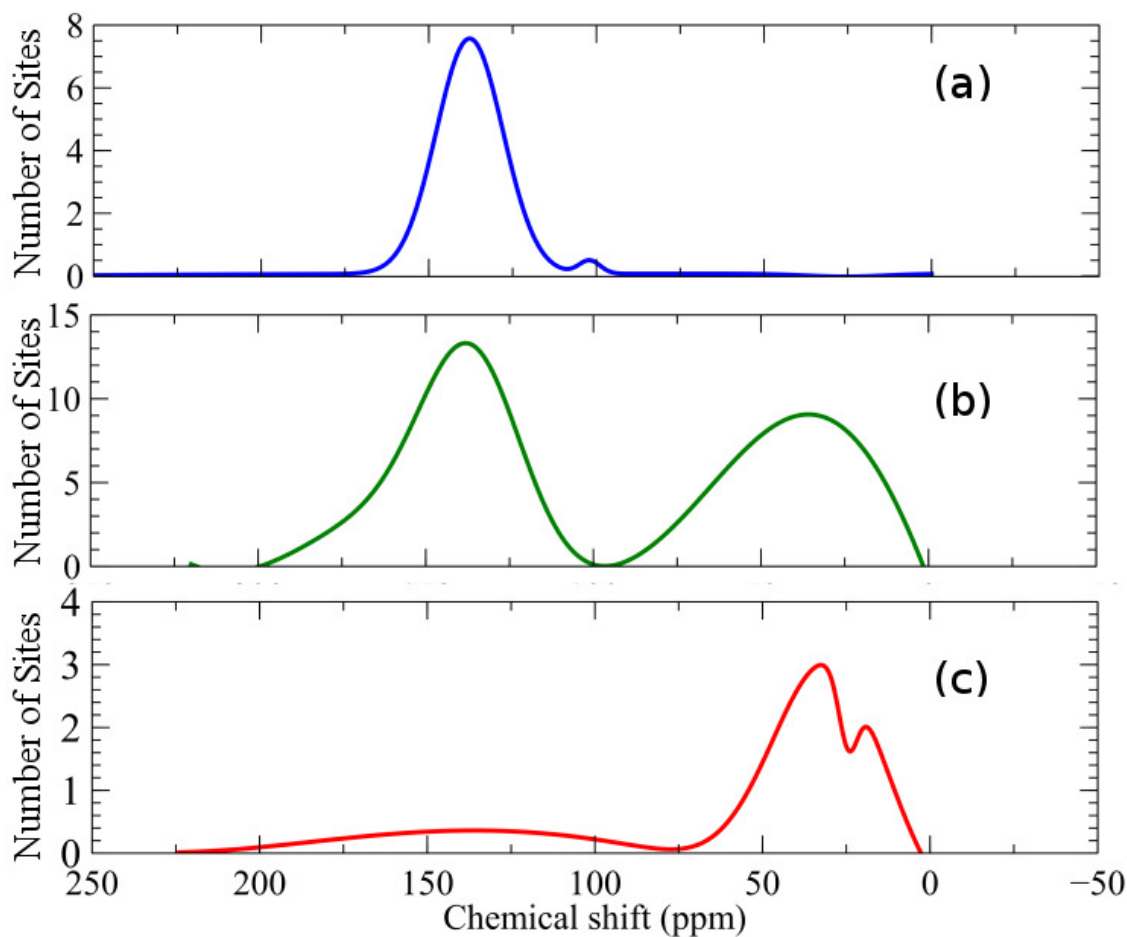
Figure 3: Calculated ^{13}C NMR spectra for systems (a) A, (b) B and (c) C.

for systems A, B and C are shown in Figure 3. The intensity (vertical axis) in these spectra is assumed to be proportional to the number of sites corresponding to each chemical shift. The histograms obtained by counting the amount of different sites according to the number and type of bonding species are shown in Figure 4, where the symbol C-C_nH_m denotes a carbon atom directly bonded to n C atoms and m H atoms. The spectra shown in Figure 3 were obtained by replacing the histograms in Figure 4 by a set of Gaussian peaks, so as to produce smooth spectra comparable to experimentally observable NMR spectra.

The spectrum obtained for system A is dominated by a chemical shift distribution with a strong peak around ~ 140 ppm, which is in good agreement with the chemical shift range expected for sp^2 carbons, as discussed in many previous reports dealing with amorphous or graphitic carbon materials.[17,19,20,22,56]

In the case of the spectrum obtained for system B, one can note that the sp^3 peak (centered around 40 ppm) becomes more intense as the H content is increased and, consequently, the H/C ratio. For a system with H/C close to 1 (which is the case of system B, as given in Table 1), the ^{13}C NMR spectrum exhibits a chemical shift distribution with the sp^2 and sp^3 peaks presenting comparable intensities, in agreement with previous experimental results obtained in carbon materials with relatively high hydrogen content.[18] In a similar way, the spectrum predicted for system C (which has an even larger H content) is dominated by a strong sp^3 peak, mostly due to C-C_2H_2 groups (in a polyethylene-like chemical environment); the sp^2 peak in this case is broader and relatively weak, which comes from the fact that the H/C ratio is higher (1.57) and system C is highly disordered, leading to a wide distribution of isotropic chemical shifts.

In amorphous hydrogenated carbon materials, the sp^2 domain sizes are expected to decrease as the H/C atomic ratio is increased, since H atoms are bonded solely to the C atoms at the edge of the sp^2 ring clusters.[57] Likewise, the sp^3 fraction is expected to grow with the increase in the H content. These trends are thus well reproduced by the NMR calculations performed for the atomistic models obtained by MD in the present work.

The width of the peak due to the sp^2 carbons (which is mainly related to the distribution of isotropic chemical shifts) is also largely affected by the sp^2 domain size, as previously discussed in the literature.[47,58] Among the obtained models, Figure 1 shows that system A exhibits the most ordered structure, composed of relatively thin aromatic layers; accordingly, the sp^2 peak is narrower in the ^{13}C NMR spectrum obtained for this system. On the other hand, system B contains small sp^2 domains (dominated by edges) and a large number of chains, whereas system C has almost isolated sp^2 groups and a small number of aromatic rings; the sp^2 peak is thus progressively broader in the ^{13}C NMR spectra predicted for systems B and C, as shown in Figure 3. The diversity of local structures is thus expected to affect the NMR lineshapes, increasing the range of chemical environments and consequently the chemical shift distribution, as reported by previous works dealing with DFT

calculations.[58]

At this point, it is worth emphasizing that the DFT calculations of the shielding tensor components here described provide information only on the contribution due to chemical shift distributions to the NMR linewidth. Other nuclear spin interactions involving dipolar couplings and bulk magnetic susceptibility effects[18] are not considered in the prediction of the NMR spectra. In the case of solid-state ^{13}C NMR spectra of carbon materials, the contributions to the linewidth due to dipolar couplings are in general minor in practical situations. This is due to two aspects: First, the heteronuclear dipolar coupling to ^1H nuclei is usually removed by high-resolution techniques commonly employed in solid-state ^{13}C NMR spectroscopy, such as MAS and high-power decoupling.[18] Furthermore, the $^{13}C-^{13}C$ homonuclear dipolar coupling is negligible in natural abundance samples, considering the low natural abundance of the ^{13}C nuclei ($\sim 1.1\%$[59]). On the other hand, the locally anisotropic diamagnetic susceptibility of graphite-like crystallites is known to cause large broadening of the resonance line associated with sp^2 carbons in materials with high degree of structural ordering.[60] Due to this kind of effect, the resonance associated with sp^2 carbons is severely broadened in graphite and in graphitic materials, notwithstanding the fact that these materials exhibit well defined chemical environments (in contrast to less ordered materials). These effects, which are thus particularly important in the ^{13}C NMR spectra of graphitic materials, are not captured by the DFT calculations of the shielding tensor here described. Therefore, one can expect that the predictions presented in Figure 3 are more likely to be comparable to experimental spectra observed for disordered materials, such as amorphous hydrogenated carbon films.[19,20,56]

The findings herein reported are also in good agreement with other first-principles studies, such as the pioneer report by Mauri *et al.*[21] In that work, the ^{13}C NMR spectra of diamond-like amorphous carbons were computed from first-principles and two different samples were considered: a hydrogenated sample, at a density of 2.2 g/cm^3, with 64 C atoms and 12 H atoms (16 at. %), in a cubic supercell; and a pure C sample, at a density of 2.9 g/cm^3,

with 64 C atoms. The chemical shift of the sp^2 peak in ref.[21] (around ~ 130 ppm) is in good agreement with the predicted chemical shifts found for systems A, B and C in the present work. As for the sp^3 peak, the calculation of ref.[21] indicates it should be located at 75 ppm, which is in good agreement with the sp^3 $C\text{-}C_4$ peak here found for model B (see Figure 4-(b)). Both the calculations reported in ref.[21] and those reported herein (for the sp^3 $C\text{-}C_4$ peak) indicate that this peak position is somewhat deviated from the chemical shift corresponding to natural diamond (~ 36 ppm.[61,62] Instead, the $C\text{-}C_4$ peak position is closer to the chemical shift corresponding to the sp^3 peak found experimentally in the ^{13}C NMR spectrum of tetrahedral amorphous carbon (ta-C), located at 69.1 ± 0.5 ppm.[22] That $ta-C$ sample presented a sp^2/sp^3 ratio of 0.22, which means that the sp^3 $C\text{-}C_4$ species are part of a matrix permeated by sp^2 clusters, consisting of aromatic rings, chains and radicals. The same can be said about the $C\text{-}C_4$ species present in systems B and C in the present work (see Figure 1). These observations thus suggest that the chemical shifts associated with carbon sites with fourfold coordination of the type $C\text{-}C_4$ are severely affected by the presence of sp^2 clusters and by the structurally disordered nature of these systems, causing a huge deviation in comparison with the chemical shift corresponding to crystalline diamond.

Chemical groups analysis

As illustrated in Figure 4 and detailed in Table 2 , the carbon sites were assorted by groups, in order to investigate the nature of the different chemical groups associated with each chemical shift range. In the distribution obtained for system A (Figure 4-(a)), there are three groups with only $C\text{-}C$ bonds: the first one is the sp^2 ($C\text{-}C_3$) peak located around 135 ppm, corresponding to quaternary carbon atoms in condensed aromatic rings; the second one is a small sp^3 ($C\text{-}C_4$) signal, located in the range 85 to 105 ppm; finally, the $C\text{-}C_2$ group chemical shifts is situated in the range 95 to 135 ppm, besides some very small signals spreading along the spectrum from 215 to 285 ppm (not shown here).

The sp^2 carbons at aromatic edges ($C\text{-}C_2H$) are the only groups with $C\text{-}H$ bonds present
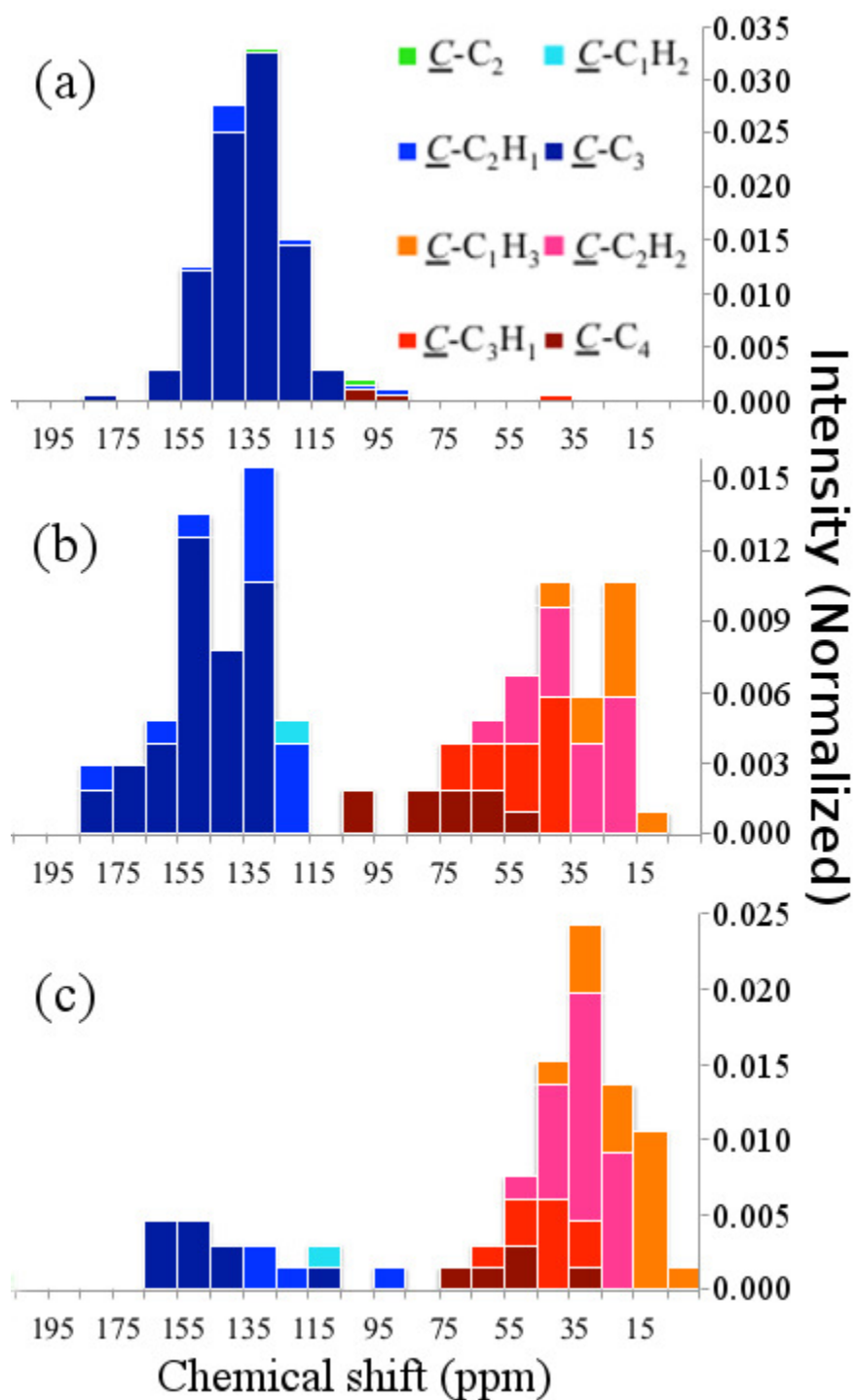
Figure 4: Histograms showing the chemical shift distribution of sites according to the number and type of bonding species, calculated for systems (a) A, (b) B and (c) C. The symbol $C\text{-}C_nH_m$ denotes a carbon atom directly bonded to n C atoms and m H atoms.

in the structure of system A; the corresponding chemical shifts appear in the range from 85 to

155 ppm. On the other hand, the chemical shift distribution obtained for system B (Figure

4-(b)) exhibits a larger number of groups containing C-H bonds. The sp^2 signal (in the range 115-185 ppm) comprises more groups of the type C-C_2H, with most of them appearing in the range 115-135 ppm, adjacent to the main C-C_3 peak (125-185 ppm). There is also a very small contribution coming from a C-CH_2 group at 122 ppm, Figure 4-(b), with only one site contributing to this signal. With respect to the sp^3 peak, there are four types of carbons: C-C_4, C-C_3H, C-C_2H_2 and C-CH_3. As expected,[21] the contribution due to C-C_4 groups is located at the extreme left-hand side of the sp^3 resonance, ranging from 45 to 105 ppm. Among those sp^3 carbons having H bonds, the C-C_2H_2 group in particular represents the largest contribution. Within this set of groups, the chemical shifts decrease when the number of H atoms increases, which is in agreement with the general trend commonly observed for ^{13}C NMR shielding in alkanes.[63,64]

In the case of system C, as illustrated in Figure 4-(c), it is observed a reduction of the sp^2 contribution intensity coming from C-C_3 and C-C_2H groups in comparison to systems A and B. The chemical shifts of the C-C_3 groups are slightly changed in position, whereas, for C-C_2H chemical shifts, displacements to lower values (85-135 ppm) are noted. Regarding the sp^3 groups, all signal intensities increase, with the exception of C-C_4 groups, which are less abundant in this hydrogen-rich system. The chemical shift range corresponding to C-C_4 groups is smaller (25-75 ppm) in comparison to systems A and B and all contributions are displaced to lower chemical shifts because of the high H content of system C.

It is important to note that the calculated distributions of chemical shifts and the predicted NMR spectra are consistent, both in shape and in terms of peak positions, with many examples of experimental ^{13}C NMR spectra of disordered carbons, such as the ^{13}C MAS experiments reported by Xu et $al.$ dealing with hydrogenated amorphous carbon coatings.[17] On the other hand, some recent assignments reported by Fedoseeva et $al.$[65] and Koroteev et $al.$[66] regarding the ^{13}C NMR spectra of ^{13}C-enriched graphitic materials are not supported at all by the present calculations. These authors have assigned signals at chemical shifts in the range 30-70 ppm to distorted sp^2-hybridized carbon atoms, whereas all results

obtained in the present calculations (and also in other previously mentioned experimental and computational investigations) indicate this chemical shift range is associated with sp^3 groups.

NMR experimental results

Besides the amorphous hydrogenated carbon films used in the comparisons between predicted and experimental NMR spectra discussed above, there are many other carbon materials whose solid-state NMR spectral features can be satisfactorily compared with the predictions presented in the previous section. Some illustrative examples of such ^{13}C NMR spectra are shown in Figure 5, where the materials analyzed include a petroleum-derived asphaltene, a peat-derived char and a pyrocarbon. By comparing the actual spectra shown in Figure 5 with the predicted spectra shown in Figure 3, it can be seen that the spectra predicted for systems A, B and C are generally comparable to the actual spectra obtained for the pyrocarbon, char and asphaltene samples, respectively. The ^{13}C NMR spectra of the asphaltene and the char show two sets of resonances, ascribed to aliphatic (chemical shifts in the range $0 - 90$ ppm) and to aromatic (chemical shifts in the range $110 - 160$ ppm) groups.[18] These distributions are quite similar to what has been found in the predicted spectra for systems B and C, where sp^3 and sp^2 groups gave contributions in the same respective chemical shift ranges.

It is worth noting that the actual distribution of number of atoms in each type of chemical environment cannot be directly computed from the relative intensities in spectra recorded with CP, as this method involves polarization transfer based on the dipolar coupling between ^{13}C and ^1H nuclei. Thus, groups with distinct dipolar couplings give rise to signals with different intensities in CP spectra, even if these groups have the same numbers of atoms.[18] However, previous reports dealing with materials containing significant amounts of hydrogen (such as humic substances, low-temperature chars and asphaltenes) have shown that, when the CP spectra are recorded using variable amplitude (VA) radiofrequency fields during the
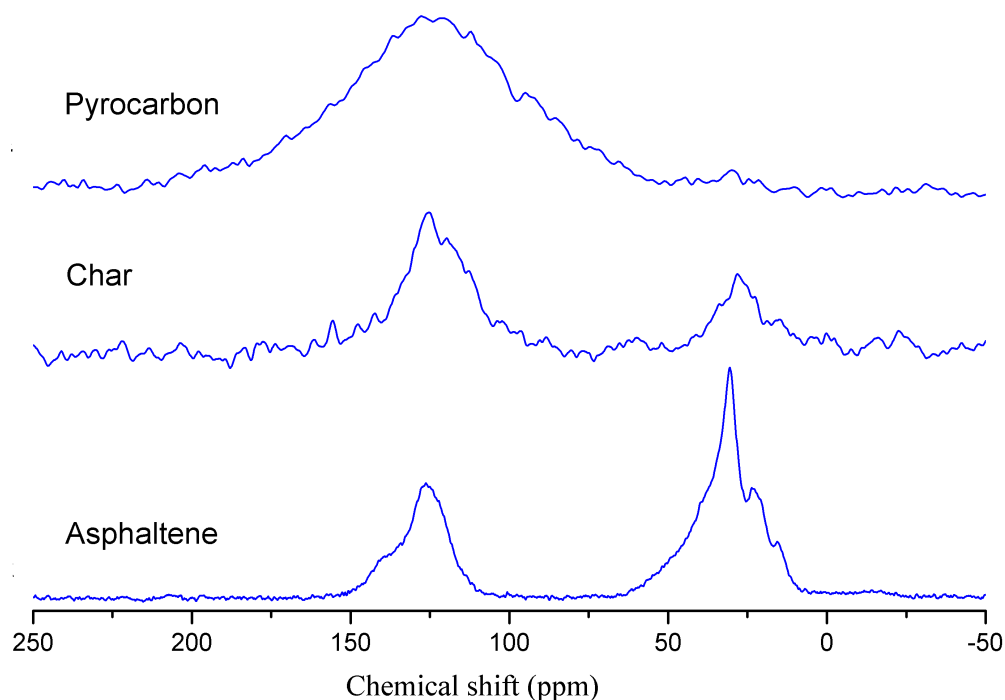
Figure 5: Experimental ^{13}C NMR spectra recorded for three examples of carbon materials (petroleum asphaltene, peat-derived char and pyrocarbon) with spectral features similar to the calculated spectra corresponding to systems A, B and C. The spectra of the char and the asphaltene sample were recorded with cross polarization, whereas the spectrum of the pyrocarbon sample was recorded using a spin-echo pulse sequence.

polarization transfer (a method known as VACP, which was indeed used in the NMR experiments here reported), no appreciable difference is observed in terms of relative intensities in comparison to truly quantitative (and more time-consuming) spectra recorded with direct polarization of ^{13}C nuclei.[18,67] Therefore, the CP spectra shown in Figure 5 can be compared in terms of general features with the predicted spectra obtained by DFT calculations using the atomistic models achieved for systems B and C. Regarding the comparison between the ^{13}C NMR spectrum calculated for system A with the experimental spectrum obtained for the pyrocarbon sample, although the peaks in both spectra (due to sp^2 carbons) appear in the same chemical shift range, the resonance width is much higher and the peak position is shifted upfield (*i.e.*, to lower chemical shifts) in the experimental case. As discussed before, this is due to the presence of graphite-like crystallites with appreciable anisotropic diamagnetic susceptibility in the pyrocarbon sample, giving rise to effects that are not completely

removed by MAS[60] and are not included in the DFT calculations used to obtain the NMR shielding. Finally, it should be emphasized that the systems simulated in the present study are composed only of H and C atoms, whereas real carbon materials are expected to contain significant amounts of heteroatoms such as O, N and S, among others. This is certainly the case of the asphaltene and the char samples whose ^{13}C NMR spectra are shown in Figure 5. It is then remarkable that the simulated spectra exhibit the same general features as the experimental ones, in terms of relative intensities and chemical shift distributions. Nevertheless, it is clear that a more refined approach is required for an improved description of the fine details of the ^{13}C NMR spectra of carbon materials containing heteroatoms. The next step in this direction, which should be pursued in future work, is the inclusion of O atoms in the modelled systems, which would be particularly important for the prediction of NMR spectral features in materials such as activated carbons and kerogens.

Conclusion

The combination of molecular dynamics and DFT was shown to be a powerful approach to generate suitable models of disordered carbons and to predict the corresponding solid-state NMR spectra. Different models were obtained starting from systems with variable H/C ratios, giving rise to final structures exhibiting different amounts of sp^3 and sp^2 carbons and distinct local structural features. The structural properties (including final densities and PDFs) were found to change drastically when the H content was varied. The ^{13}C NMR spectra were predicted by DFT/GIPAW calculations of the shielding tensors corresponding to each atomic site and were analyzed considering the distributions of chemical shifts associated with each type of neighborhood around those sites. This method of analysis distinguishing the different types of chemical environments can be very useful for analyzing and labeling the several signals present in the solid-state NMR spectra of disordered carbons. The predicted NMR spectra were satisfactorily compared with experimental results avail-

able for amorphous hydrogenated carbon films; the comparison was also extended to NMR spectra recorded for some representative carbon materials (including an asphaltene, a char and a pyrocarbon), with a good agreement also observed in this case, even though the real materials are chemically more complex than the simulated systems. The present results offer then a basis for the construction of more realistic models including other chemical species, which can be used for the prediction of structural and spectral features of materials such as kerogens and activated carbons.

Acknowledgement

References

(1) Oberlin, A.; Bonnamy, S. A Realistic Approach to Disordered Carbons. Chemistry & Physics of Carbon. Series: Chemistry and Physics of Carbon, CRC Press, Edited by Ljubisa Radovic **2012**, 1–84.

(2) Leyssale, J.-M.; Da Costa, J.-P.; Germain, C.; Weisbecker, P.; Vignoles, G. Structural Features of Pyrocarbon Atomistic Models Constructed from Transmission Electron Microscopy Images. Carbon **2012**, 50, 4388–4400.

(3) Vignoles, G. L.; Lachaud, J.; Aspa, Y.; Goyhénèche, J.-M. Ablation of Carbon-Based Materials: Multiscale Roughness Modelling. Compos. Sci. Technol. **2009**, 69, 1470–1477.

(4) Ewels, C.; Heggie, M.; Briddon, P. Adatoms and Nanoengineering of Carbon. Chem. Phys. Lett. **2002**, 351, 178–182.

(5) Opletal, G.; Drumm, D. W.; Wang, R. P.; Russo, S. P. Structural Modeling of $Ge_{6.25}As_{32.5}Se_{61.25}$ Using a Combination of Reverse Monte Carlo and Ab Initio Molecular Dynamics. J. Phys. Chem. A **2014**, 118, 4790–4796.

(6) Stratford, J. M.; Mayo, M.; Allan, P. K.; Pecher, O.; Borkiewicz, O. J.; Wiaderek, K. M.; Chapman, K. W.; Pickard, C. J.; Morris, A. J.; Grey, C. P. Investigating Sodium Storage Mechanisms in Tin Anodes: A Combined Pair Distribution Function Analysis, Density Functional Theory, and Solid-State NMR Approach. J. Am. Chem. Soc. **2017**, 139, 7273–7286.

(7) Bousige, C.; Ghimbeu, C. M.; Vix-Guterl, C.; Pomerantz, A. E.; Suleimenova, A.; Vaughan, G.; Garbarino, G.; Feygenson, M.; Wildgruber, C.; Ulm, F.-J., et al. Realistic Molecular Model of Kerogen's Nanostructure. Nat. Mater. **2016**, 15, 576.

(8) Ponomarev, I.; Kroll, P. 29Si NMR Chemical Shifts in Crystalline and Amorphous Silicon Nitrides. Materials **2018**, 11.

(9) Ferreira, A. R.; Rino, J. P. On the Use of Atomistic Simulations to Aid Bulk Metallic Glasses Structural Elucidation with Solid-State NMR. Sci. Rep. **2017**, 7, 9305.

(10) Marín-Luna, M.; Claramunt, R. M.; Nieto, C. I.; Alkorta, I.; Elguero, J.; Reviriego, F. A theoretical NMR Study of Polymorphism in Crystal Structures of Azoles and Benzazoles. Magn. Reson. Chem. **2019**, 57, 275–284.

(11) Zurek, E.; Pickard, C. J.; Autschbach, J. Density Functional Study of the 13C NMR Chemical Shifts in Single-Walled Carbon Nanotubes with Stone- Wales Defects. J. Phys. Chem. C **2008**, 112, 11744–11750.

(12) Casabianca, L. B.; Shaibat, M. A.; Cai, W. W.; Park, S.; Piner, R.; Ruoff, R. S.; Ishii, Y. NMR-Based Structural Modeling of Graphite Oxide Using Multidimensional 13C Solid-State NMR and Ab Initio Chemical Shift Calculations. J. Am. Chem. Soc. **2010**, 132, 5672–5676.

(13) Vähäkangas, J.; Ikäläinen, S.; Lantto, P.; Vaara, J. Nuclear Magnetic Resonance Predictions for Graphenes: Concentric Finite Models and Extrapolation to Large Systems. Phys. Chem. Chem. Phys. **2013**, 15, 4634–4641.

(14) de Souza, F. A. L.; Ambrozio, A. R.; Souza, E. S.; Cipriano, D. F.; Scopel, W. L.; Freitas, J. C. C. NMR Spectral Parameters in Graphene, Graphite, and Related Materials: Ab Initio Calculations and Experimental Results. J. Phys. Chem. C **2016**, 120, 27707–27716.

(15) Mathioudakis, C.; Kopidakis, G.; Kelires, P.; Wang, C.; Ho, K. Physical Trends in Amorphous Carbon: a Tight-Binding Molecular-Dynamics Study. Phys. Rev. B **2004**, 70, 125202.

(16) Erdemir, A.; Donnet, C. Tribology of Diamond-Like Carbon Films: Recent Progress and Future Prospects. J. Phys. D Appl. Phys. **2006**, 39, R311–R327.

(17) Xu, J.; Watanabe, S.; Hayashi, H.; Kawaguchi, M.; Kato, T. Structural Characterization of Ion-Vapor Deposited Hydrogenated Amorphous Carbon Coatings by Solid State 13C Nuclear Magnetic Resonance. J. Appl. Phys. **2014**, 115, 014303.

(18) Freitas, J. C. C.; Cunha, A. G.; Emmerich, F. G. Chem. Phys. Carbon; CRC Press, 2012; pp 102–187.

(19) Pan, H.; Pruski, M.; Gerstein, B.; Li, F.; Lannin, J. S. Local Coordination of Carbon Atoms in Amorphous Carbon. Phys. Rev. B **1991**, 44, 6741.

(20) Cho, G.; Yen, B. K.; Klug, C. A. Structural Characterization of Sputtered Hydrogenated Amorphous Carbon Films by Solid State Nuclear Magnetic Resonance. J. Appl. Phys. **2008**, 104, 013531.

(21) Mauri, F.; Pfrommer, B. G.; Louie, S. G. Ab Initio NMR Chemical Shift of Diamond, Chemical-Vapor-Deposited Diamond, and Amorphous Carbon. Phys. Rev. Lett. **1997**, 79, 2340.

(22) Alam, T. M.; Friedmann, T.; Schultz, P. A.; Sebastiani, D. Low Temperature Annealing in Tetrahedral Amorphous Carbon Thin Films Observed by 13C NMR Spectroscopy. Phys. Rev. B **2003**, 67, 245309.

(23) Mohr, S.; Ratcliff, L. E.; Genovese, L.; Caliste, D.; Boulanger, P.; Goedecker, S.; Deutsch, T. Accurate and Efficient Linear Scaling DFT Calculations with Universal Applicability. Phys. Chem. Chem. Phys. **2015**, 17, 31360–31370.

(24) Mohr, S.; Eixarch, M.; Amsler, M.; Mantsinen, M. J.; Genovese, L. Linear scaling DFT calculations for large Tungsten systems using an optimized local basis. Nucl. Mater. Energy **2018**, 15, 64–70.

(25) Obliger, A.; Valdenaire, P.-L.; Capit, N.; Ulm, F. J.; Pellenq, R. J.-M.; Leyssale, J.-M. Poroelasticity of Methane-Loaded Mature and Immature Kerogen from Molecular Simulations. Langmuir **2018**, 34, 13766–13780.

(26) Srinivasan, S. G.; Van Duin, A. C.; Ganesh, P. Development of a ReaxFF potential for Carbon Condensed Phases and its Application to the Thermal Fragmentation of a Large Fullerene. J. Phys. Chem. A **2015**, 119, 571–580.

(27) Van Duin, A. C.; Dasgupta, S.; Lorant, F.; Goddard, W. A. ReaxFF: A reactive Force Field for Hydrocarbons. J. Phys. Chem. A **2001**, 105, 9396–9409.

(28) Chenoweth, K.; Van Duin, A. C.; Goddard, W. A. ReaxFF Reactive Force Field for Molecular Dynamics Simulations of Hydrocarbon Oxidation. J. Phys. Chem. A **2008**, 112, 1040–1053.

(29) Plimpton, S. Fast Parallel Algorithms for Short-Range Molecular Dynamics. J. Comput. Phys. **1995**, 117, 1–19.

(30) Swope, W. C.; Andersen, H. C.; Berens, P. H.; Wilson, K. R. A computer simulation method for the calculation of equilibrium constants for the formation of physical clusters of molecules: Application to small water clusters. J. Chem. Phys. **1982**, 76, 637–649.

(31) Nosé, S. A Unified Formulation of the Constant Temperature Molecular Dynamics Methods. J. Chem. Phys. **1984**, 81, 511–519.

(32) Hoover, W. G. Canonical Dynamics: Equilibrium Phase-Space Distributions. Phys. Rev. A **1985**, 31, 1695–1697.

(33) Giannozzi, P.; Baroni, S.; Bonini, N.; Calandra, M.; Car, R.; Cavazzoni, C.; Ceresoli, D.; Chiarotti, G. L.; Cococcioni, M.; Dabo, I., et al. QUANTUM ESPRESSO: A Modular and Open-Source Software Project for Quantum Simulations of Materials. J. Phys. Condens. Matter. **2009**, 21, 395502.

(34) Pickard, C. J.; Mauri, F. All-Electron Magnetic Response with Pseudopotentials: NMR Chemical Shifts. Phys. Rev. B **2001**, 63, 245101.

(35) Blöchl, P. E. Projector Augmented-Wave Method. Phys. Rev. B **1994**, 50, 17953.

(36) Mauri, F.; Pfrommer, B. G.; Louie, S. G. Ab Initio Theory of NMR Chemical Shifts in Solids and Liquids. Phys. Rev. Lett. **1996**, 77, 5300.

(37) Mauri, F.; Louie, S. G. Magnetic Susceptibility of Insulators from First Principles. Phys. Rev. Lett. **1996**, 76, 4246.

(38) Perdew, J. P.; Burke, K.; Ernzerhof, M. Generalized Gradient Approximation Made Simple. Phys. Rev. Lett. **1996**, *77*, 3865–3868.

(39) Troullier, N.; Martins, J. L. Efficient Pseudopotentials for Plane-Wave Calculations. Phys. Rev. B **1991**, *43*, 1993.

(40) Grimme, S.; Ehrlich, S.; Goerigk, L. Effect of the Damping Function in Dispersion Corrected Density Functional Theory. J. Comput. Chem. **2011**, *32*, 1456–1465.

(41) Zurek, E.; Pickard, C. J.; Walczak, B.; Autschbach, J. Density Functional Study of the 13C NMR Chemical Shifts in Small-to-Medium-Diameter Infinite Single-Walled Carbon Nanotubes. J. Phys. Chem. A **2006**, *110*.

(42) Marques, M. A. L.; d'Avezac, M.; Mauri, F. Magnetic Response and NMR Spectra of Carbon Nanotubes from Ab Initio Calculations. Phys. Rev. B **2006**, *73*, 125433.

(43) Jameson, A.; Jameson, C. J. Gas-Phase 13C Chemical Shifts in the Zero-Pressure Limit: Refinements to the Absolute Shielding Scale for 13C. Chem. Phys. Lett. **1987**, *134*, 461–466.

(44) da Silva Oliveira, E. C.; Álvaro Cunha Neto,; Júnior, V. L.; de Castro, E. V. R.; de Menezes, S. M. C. Study of Brazilian Asphaltene Aggregation by Nuclear Magnetic Resonance spectroscopy. Fuel **2014**, *117*, 146–151.

(45) Freitas, J. C. C.; Bonagamba, T. J.; Emmerich, F. G. 13C High-Resolution Solid-State NMR Study of Peat Carbonization. Energy Fuels **1999**, *13*, 53–59.

(46) Farbos, B.; Weisbecker, P.; Fischer, H. E.; Da Costa, J.-P.; Lalanne, M.; Chollon, G.; Germain, C.; Vignoles, G. L.; Leyssale, J.-M. Nanoscale structure and texture of highly anisotropic pyrocarbons revisited with transmission electron microscopy, image processing, neutron diffraction and atomistic modelings. Carbon **2014**, *80*, 472–489.

(47) Forse, A. C.; Merlet, C.; Allan, P. K.; Humphreys, E. K.; Griffin, J. M.; Aslan, M.; Zeiger, M.; Presser, V.; Gogotsi, Y.; Grey, C. P. New Insights into the Structure of Nanoporous Carbons from NMR, Raman, and Pair Distribution Function Analysis. Chem. Mater. **2015**, 27, 6848–6857.

(48) Weisbecker, P.; Leyssale, J.-M.; Fischer, H. E.; Honkimäki, V.; Lalanne, M.; Vignoles, G. L. Microstructure of Pyrocarbons from Pair Distribution Function Analysis Using Neutron Diffraction. Carbon **2012**, 50, 1563–1573.

(49) Krainyukova, N. V.; Zubarev, E. N. Carbon Honeycomb High Capacity Storage for Gaseous and Liquid Species. Phys. Rev. Lett. **2016**, 116, 055501.

(50) Andrews, A. B.; Edwards, J. C.; Pomerantz, A. E.; Mullins, O. C.; Nordlund, D.; Norinaga, K. Comparison of Coal-Derived and Petroleum Asphaltenes by 13C Nuclear Magnetic Resonance, DEPT, and XRS. Energy Fuels **2011**, 25, 3068–3076.

(51) Van Krevelen, D. W. Coal: Typology, Physics, Chemistry, Constitution; Elsevier Amsterdam, 1993.

(52) Iarlori, S.; Galli, G.; Martini, O. Microscopic Structure of Hydrogenated Amorphous Carbon. Phys. Rev. B **1994**, 49, 7060–7063.

(53) Newport, R.; Honeybone, P.; Cottrell, S.; Franks, J.; Revell, P.; Cernik, R.; Howells, W. The Structure of a C:H by Neutron and X-Ray Scattering. Surf. Coat. Tech. **1991**, 47, 668–676.

(54) Allen, F. H.; Kennard, O.; Watson, D. G.; Brammer, L.; Orpen, A. G.; Taylor, R. Tables of Bond Lengths Determined by X-ray and Neutron Diffraction. Part 1. Bond Lengths in Organic Compounds. J. Chem. Soc., Perkin Trans. 2 **1987**, S1–S19.

(55) Costain, C. C.; Stoicheff, B. P. Microwave Spectrum, Molecular Structure of Vinyl

Cyanide and a Summary of CC, CH Bond Lengths in Simple Molecules. J. Chem. Phys. **1959**, 30, 777–782.

(56) Chu, P. K.; Li, L. Characterization of Amorphous and Nanocrystalline Carbon Films. Mater. Chem. Phys. **2006**, 96, 253–277.

(57) Koidl, P.; Wild, C.; Dischler, B.; Wagner, J.; Ramsteiner, M. Plasma Deposition, Properties and Structure of Amorphous Hydrogenated Carbon Films. Properties and Characterization of Amorphous Carbon Films. 1991; pp 41–70.

(58) Forse, A. C.; Griffin, J. M.; Presser, V.; Gogotsi, Y.; Grey, C. P. Ring Current Effects: Factors Affecting the NMR Chemical Shift of Molecules Adsorbed on Porous Carbons. J. Phys. Chem. C **2014**, 118, 7508–7514.

(59) Harris, R. K.; Becker, E. D.; De Menezes, S. M. C.; Goodfellow, R.; Granger, P. NMR Nomenclature. Nuclear Spin Properties and Conventions for Chemical Shifts (IUPAC Recommendations 2001). Pure Appl. Chem. **2001**, 73, 1795–1818.

(60) Freitas, J. C.; Emmerich, F. G.; Cernicchiaro, G. R.; Sampaio, L. C.; Bonagamba, T. J. Magnetic Susceptibility Effects on 13C MAS NMR Spectra of Carbon Materials and Graphite. Solid State Nucl. Magn. Reson. **2001**, 20, 61–73.

(61) Merwin, L. H.; Johnson, C. E.; Weimer, W. A. 13C NMR Investigation of CVD Diamond: Correlation of NMR and Raman Spectral Linewidths. J. Mater. Res. **1994**, 9, 631–635.

(62) Wilkie, C. A.; Ehlert, T. C.; Haworth, D. T. A Solid State 13C-NMR Study of Diamonds and Graphites. J. Inorg. Nucl. Chem. **1978**, 40, 1983 – 1987.

(63) Grant, D. M.; Paul, E. G. Carbon-13 Magnetic Resonance. II. Chemical Shift Data for the Alkanes. J. Am. Chem. Soc. **1964**, 86, 2984–2990.

(64) d'Antuono, P.; Botek, E.; Champagne, B.; Spassova, M.; Denkova, P. Theoretical Investigation on H1 and C13 NMR Chemical shifts of Small Alkanes and Chloroalkanes. J. Chem. Phys **2006**, _125_, 144309.

(65) Fedoseeva, Y. V.; Okotrub, A.; Koroteev, V.; Borzdov, Y. M.; Palyanov, Y. N.; Shubin, Y. V.; Maksimovskiy, E.; Makarova, A.; Münchgesang, W.; Bulusheva, L., et al. Graphitization of 13C Enriched Fine-Grained Graphitic Material Under High-Pressure Annealing. Carbon **2019**, _141_, 323–330.

(66) Koroteev, V.; Münchgesang, W.; Shubin, Y. V.; Palyanov, Y. N.; Plyusnin, P.; Smirnov, D.; Kovalenko, K.; Bobnar, M.; Gumeniuk, R.; Brendler, E., et al. Multiscale characterization of 13C-enriched fine-grained graphitic materials for chemical and electrochemical applications. Carbon **2017**, _124_, 161–169.

(67) Novotny, E. H.; Hayes, M. H.; Bonagamba, T. J., et al. Characterisation of Black Carbon-Rich Samples by 13C Solid-State Nuclear Magnetic Resonance. Naturwissenschaften **2006**, _93_, 447–450.

1
2
3
4
5
6
7
8
9
10
11
12
13
14
15
16
17
18
19
20
21
22
23
24
25
26
27
28
29
30
31
32
33
34
35
36
37
38
39
40
41
42
43
44
45
46
47
48
49
50
51
52
53
54
55
56
57
58
59
60

Graphical TOC Entry